האגוד הישראלי למכניקה עיונית ושימושית

The Israel Society for Theoretical and Applied Mechanics

ISTAM

An Adhering Organization of the
International Union of Theoretical and Applied Mechanics
(IUTAM: http://www.iutam.net**)**

ISTAM Annual Symposium

TECHNICAL PROGRAM

28 December 2008

Tel Aviv University

ISTAM Annual Symposium

28 December 2008

TECHNICAL PROGRAM

Location: Rosenblatt Auditorium, Computer and Software Engineering Building, Tel Aviv University

09:30 – 09:50 Registration and coffee

09:50 – 10:00 *Opening:* MB Rubin, Technion, President of ISTAM

Morning Session Chairman: G deBotton, Ben-Gurion University

10:00 – 10:30 **C Sansour**, S Skatulla, A Arunachalakasi, University of Nottingham. *Electro-mechanically coupled deformations within the framework of generalised continua*

10:30 – 11:00 **B Nadler**. University of Alberta. *Decohesion of nonlinear membrane*

11:00 – 11:30 **I Einav**, University of Sydney. *Continuum comminution theory of confined granular materials*

11:30 – 12:00 **E Bouchbinder**, A Livne and J Fineberg, Hebrew University. *Elastic non-linearities in dynamic fracture*

12:00 – 12:30 **E Levenberg,** Purdue University. *Simultaneous application of creep and relaxation formulations to study nonlinear behavior of particle-reinforced viscoelastic composites*

12:30 – 14:00 Lunch (The registration fee includes lunch)

Afternoon Session Chairman: I Goldhirsch, Tel Aviv University

14:00 – 14:30 Leopold Grinberg, **A Yakhot,** GE Karniadakis, Ben-Gurion University. *Analyzing Transient Turbulence in a Stenosed Carotid Artery by Proper Orthogonal Decomposition*

14:30 – 15:00 **L Shemer**, Tel-Aviv University. *Rogue (Freak) Waves in Ocean and in a Laboratory Tank*

15:00 – 15:30 **KY Volokh,** Technion. *Transition to turbulence through decline of viscosity*

15:30 – 16:00 **T Cohen**, D Durban, Technion. *Plane stress cavitation in elastic solids*

The annual membership fee to ISTAM is 60 NIS. It includes the lunch at the symposium and can be paid during the registration.

All lectures are open to the public free of charge

Electro-mechanically coupled deformations within the framework of generalised continua

C Sansour, S Skatulla, A Arunachalakasi

Division of Materials, Mechanics, and Structures, Faculty of Engineering,
University of Nottingham, UK
Email: carlo.sansour@nottingham.ac.uk

Materials exhibiting electro-mechanically coupled behaviour, such as ferroelectrics, magnetostrictive materials, or electro-active polymers (EAP), belong to the group of so-called smart materials. The nonlinear behaviour of ferroelectrics and magnetosrtictive materials, however, is not fully understood, which considerably limits their range of application to the small displacement regime. Beyond this regime hysteresis and nonlinearity characterise the material behaviour and the rate of loading becomes crucial under such conditions. On the other hand EAP have the characteristic to undergo large deformations while sustaining correspondingly large electrical loading. This latter property can be utilized for actuators in electro-mechanical systems, artificial muscles and so forth.

The electromechanical behaviour is described within the framework of generalised continua. Such an approach provides naturally the degree of freedom which is work conjugate to an external moment, a type of loading which is present in electromechanical coupled phenomena. Moreover, it also provides a scale effect which is of importance at micro scales and affects the behaviour of micromechanical devices. In addition, a new and physically appealing formulation for EAP will be given.

The above theories will be put to the test via finite element and meshfree formulations. Various computations of hysteresis effects in ferroelectrics as well as large deformations of EAP devices will be discussed.

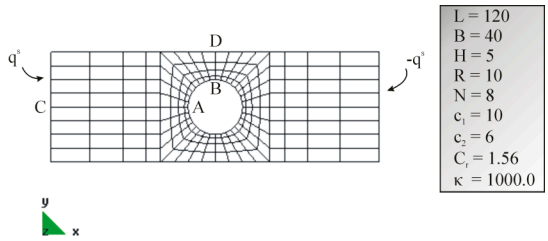

Fig. 1: Problem definition of a plate with a circular hole subjected to surface charge loading

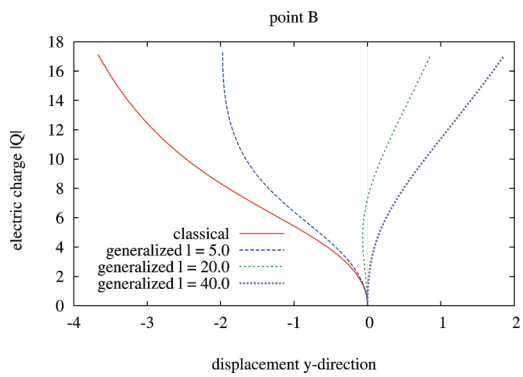

Fig. 2: Load displacement graph illustrating the contraction or expansion of the hole in y-direction

The problem being investigated is a plate with a hole at its centre subjected to electric surface charge loading q^s as depicted in Fig. 1. The meshfree particle distribution corresponds to the illustrated mesh. On application of the electric surface charge loading an electric field develops which leads to contraction of the plate in x-coordinate direction. In graph Fig. 2 the displacement in y-direction versus electric surface charge loading at point B is illustrated. The classical solution is denoted by the red line and the generalized solutions are modelled assuming a two-dimensional micro-space with its directors being parallel to the x- and y-coordinate axes. Three different scaling levels are investigated firstly, choosing the internal length scale parameters $l = l_x = l_y = 5.0$ denoted by the blue line, secondly, $l = l_x = l_y = 20.0$ denoted by the green line, and thirdly, $l = l_x = l_y = 40.0$ denoted by the purple line. The transition to the classical solution is achieved by setting the internal length scale parameters to very small values $l = l_x = l_y < 10^{-3}$. For this case the strain gradient contribution is negligible small and the conventional part of the proposed problem formulation is dominant. An interesting effect can be observed that, in contrast to the classical result, where the hole is contracting, for the two highest scaling levels the diameter of the hole is actually expanding in y-coordinate direction.

References

[1] S. Skatulla, A. Arunachalakasi, and C. Sansour (2008), A nonlinear generalized continuum approach for electro-elasticity including scale effects, J Mechanics Physics Solids, in print, available online.

[2] A. Arockiarajan and C. Sansour (2008), Micromechanical modeling and simulation of rate-dependent effects in ferroelectric polycrystals, Computational Materials Science 43, 842-854.

Decohesion of nonlinear membrane

Ben Nadler

Faculty of Mechanical Engineering, University of Alberta
Edmonton, AB, Canada. Email: bnadler@ualberta.ca

Adhesion of flexible thin film or membrane is important to a variety of biological and industrial applications. For example, membrane-membrane adhesion is prominent to cell and vesicle aggregation. Spreading and attachment of cells to extracellular matrix (ECM) is crucial for the survival, proliferation and differentiation of cells. Regulation of cell activities can therefore be achieved by modulating the binding of the cell to ECM using chemical or mechanical controls. Bacteria form biofilm and adhere to surfaces, causing biofouling - a serious environmental and industrial problem. Moreover, performance of many submicron electromechanical systems may also be compromised due to collapse and sticking of thin films onto substrates.

Many experimental techniques and theoretical models have been developed to characterize the elastic response and adhesion of a flexible thin film or membrane. All previous works are based on linear elasticity and assumption of small deformation. In many physical systems, however, large deformation is often expected, especially for biological membranes. The question of whether the debonding process obtained from a nonlinear analysis differs from the linear elastic solution is the motivation of this work.

In this work, we assume the membrane is nonlinear elastic. Without assuming small deformation, we present a formulation to capture the decohesion process. In the case of initially stress free membrane, our results exhibit qualitatively similar behavior to the linear elasticity model of failure, but the critical contact radius at pull-off is found to be dependent on the material constant. Further study on the effect of prestresses shows that the pull-off load and critical contact radius do not vary monotonically with the magnitude of the prestress. This surprising difference from the linear elastic solution suggests that large deformation can have a significant effect on membrane adhesion and should be taken into consideration.

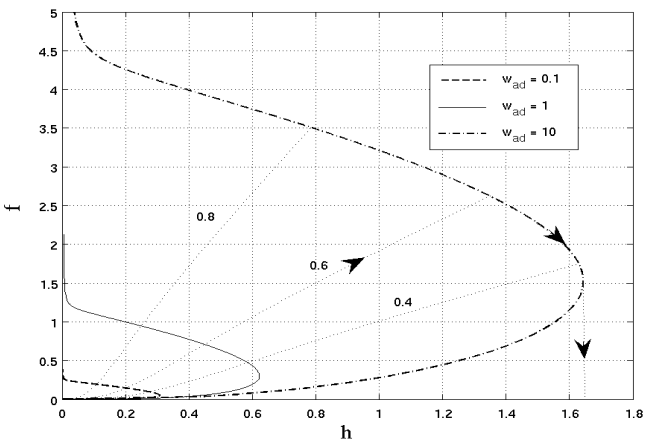

Loading path envelops satisfying fracture condition.

Keywords: *Membranes; Adhesion; Decohesion, Finite deformation.*

Reference:

[1] B. Nadler and T. Tian, (2008) Decohesion of a rigid punch from nonlinear membrane undergoing finite axisymmetric deformation, *Int. J. Non-linear Mech.* 43*, 716-721.*

Continuum comminution theory of confined granular materials

Itai Einav

School of Civil Engineering
Faculty of Engineering & IT, University of Sydney
NSW 2006, Australia. Email: i.einav@civil.usyd.edu.au URL: http://www.civil.usyd.edu.au/

Comminution is the process of grain-size reduction through crushing, cutting, breaking and grinding. It is pivotal to many operations in many industries, including mineral processing, agriculture, pharmaceutics, and in geoscience. 'Confined comminution' occurs in constrained processes such as the constrained flow of particles against solid surfaces in industrial mills, and sand production from oil-producing perforations, and the motion of rocks in fault gouges (cataclasis).

For more than a century, theories of comminution have been studied in terms of the energy consumed during the operation of mills. Subsequent models of comminution have refined the predictive capabilities of these early works for specific circumstances. Each of these models can be calibrated to fit predictions of the change in grain-size distribution (gsd) during a particular operation. However, their fit is extremely sensitive to changes in geometrical constraints of an operation. A continuum mechanics theory of comminution is therefore required, since it may embrace through a single constitutive model the required ingredients for predicting how the gsd evolves in response to stress-strain variations, at any point in the problem domain, without recalibrating the model to changes in the boundary conditions.

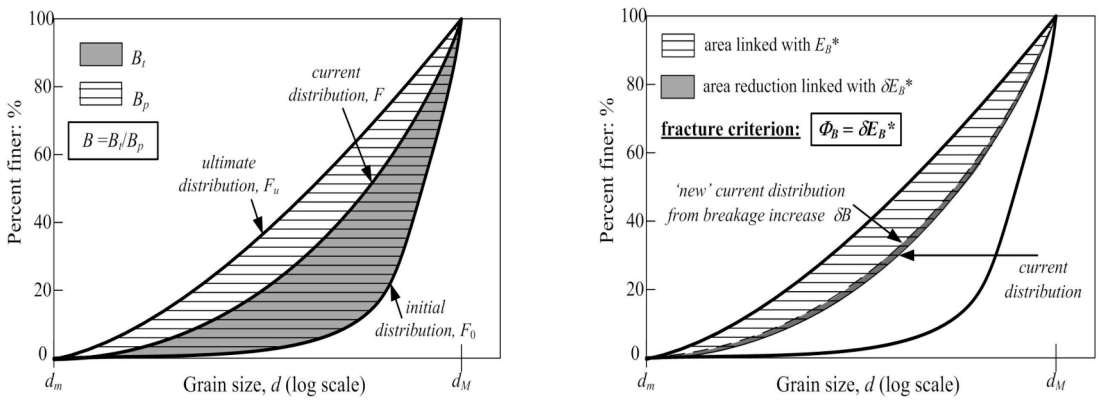

Figure 1. The breakage measurement and evolution law (Einav, 2007a,b). The left figure (a) portrays the measurable definition of breakage, B, in terms of the initial, current and ultimate grain size distributions. The right diagram (b) presents the breakage propagation criterion for granular materials. Φ_B is the breakage dissipation, denoting the energy consumption from incremental increase of breakage. δE_B^* is the incremental reduction in the residual breakage energy. The energy balance equation, $\Phi_B = \delta E_B^*$, was shown to produce a physical evolution law for B.

This talk will present first principles of thermodynamics for the characterization of brittle granular materials, which enables to link the stress-strain relations to the evolution of the gsd. The result is a constitutive theory of comminution, termed Breakage Mechanics (Einav, 2007a). In this theory, a single measurable internal variable is introduced, i.e. the breakage, which scales the distance of the current gsd from a reference initial gsd and an ultimate gsd (see Fig. 1a). Focus will be given to exploring the physics of brittle granular compaction, which provides the backbone for the evolution equations. Connections to Griffith's energy method for cracks under tension will follow (Einav, 2007b) (see Fig. 1b). We will investigate the behaviour of brittle granular mixtures, i.e., materials with mixed particles from two or more minerals, through a separate mixture theory (Einav & Valdes, 2008). Then new ideas will be placed forward that show how the single breakage variable could be replaced by the entire gsd through variational principles. A short discussion will then follow, presenting the treatment of shear deformations.

References

[1] Einav I, 2007a. Breakage mechanics. Part I- theory. *J. Mech. Phys. Solids*. **55**(6), 1274-1297. Breakage mechanics. Part II: Modelling granular materials. *J. Mech. Phys. Solids*. **55**(6), pp., 1298-1320.

[2] Einav I. 2007b. Fracture propagation in brittle granular matter. *Proc. Roy. Soc. A.* 463, 2087, pp., 3021-3035.

[3] Einav I., Valdes J. 2008. On comminution and yield in brittle granular mixtures. *J. Mech. Phys. Solids.* 56(6), 2136-2148.

Elastic non-linearities in dynamic fracture

Eran Bouchbinder, Ariel Livne and Jay Fineberg

Racah Institute of Physics, Hebrew University of Jerusalem, Jerusalem 91904, Israel
Email: eran.bouchbinder@weizmann.ac.il

The classic approach to crack dynamics, linear elastic fracture mechanics (LEFM), predicts a $r^{-1/2}$ strain and stress divergence at a crack tip. This significant stress enhancement is commonly assumed to drive material failure at small scales in the immediate vicinity of the tip of a crack. However, as real materials can not support diverging stresses, these stresses are regularized within a small region, the process zone, that surrounds a crack's tip. Understanding the near-tip structure of a crack is of enormous importance, as how a material regularizes the stress singularity at a crack's tip will determine whether its failure is rapid and cataclysmic, as in brittle materials, or of a gradual, flowing character, as in ductile ones.

Progress in understanding the process zone structure has, on the whole, been limited by our lack of hard data describing the detailed physical processes that occur within the process zone. Due to its generally microscopic size and high propagation velocity (near sound speed), the dynamical behavior of this elusive region has never before been directly observed in dynamic fracture, hence numeric or atomistic calculations have been the sole quantitative means to access it. Here we present a combined experimental and theoretical dynamic fracture study of the breakdown of LEFM and the emergence of nonlinear elastic effects as the process zone is approached. We derive the leading nonlinear elastic corrections to LEFM, resulting in strain contributions "more-divergent" than $r^{-1/2}$ at a finite distance from the tip and logarithmic corrections to the parabolic crack tip opening displacement. In addition, a dynamic length-scale, associated with the nonlinear elastic zone, emerges naturally.

The theory provides excellent agreement with direct near-tip measurements that can not be described in the LEFM framework. These results provide a first-principles description the weakly nonlinear elastic region that resides within the process zone. We propose that the nonlinear elastic region, that bridges the gap between LEFM and the dissipative region may play a critical role in governing the fracture process. Thus, our results may be a first step in unlocking a plethora of open questions that are related to instabilities of single straight cracks.

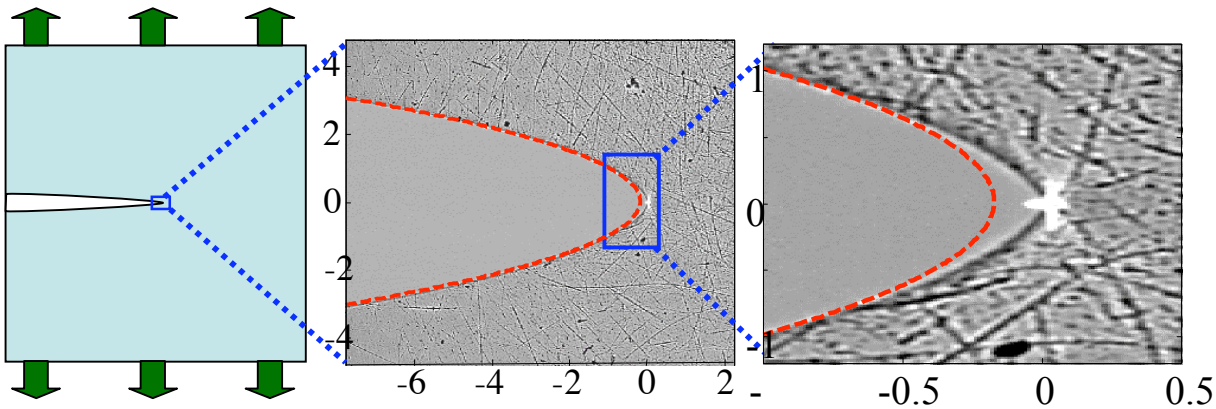

Fig. 1: (Left) A sketch of the experimental setup. (Middle) Zoom in on the crack tip region. The red dashed line is a parabolic fit to the crack tip opening displacement, following the LEFM prediction. The random scratches pattern provides us with an effective particles tracking technique that allows a direct measurement of the deformation in the near tip vicinity. (Right) Further zooming in on the crack tip. A deviation from the LEFM parabolic profile is observed. All axes are measured in mm.

The fracture of polyacrylamide gels has provided a vehicle for directly observing the detailed dynamics of rapid crack propagation. By slowing the process down by nearly three orders of magnitude, experiments have demonstrated tensile cracks propagating in this brittle neo-Hookean material have dynamics which are identical to those of other amorphous brittle materials. These correspond to both single-crack dynamics predicted by linear elastic fracture mechanics (LEFM) as well as crack instabilities at high crack propagation velocities.

Figure 1 shows photographs of the near tip region and illustrates the idea behind the particles tracking method that allows a direct measurement of the deformation near a running crack tip. A parabolic fit to the crack opening displacement is added and a deviation from it is observed. Figure 2 shows the measured tensile strain component ahead of the crack tip, as well as the LEFM and the weakly nonlinear theory predictions. It is shown that while LEFM fails to describe the measured data, where the discrepancies grow with increasing crack velocity, the weakly nonlinear theory provides an accurate description of the data.

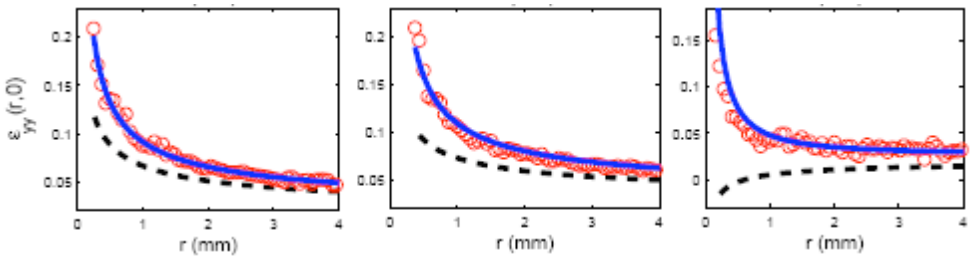

Fig. 2: (Left) The red circles are the measured tensile strain component ahead of the crack tip for v=0.20Cs, where Cs is the shear wave speed. r is the distance measured from the tip. The black dashed line is the LEFM prediction, while the blue line is the prediction of the weakly nonlinear theory. (Middle) The same, but for v=0.53Cs (Right) The same, but for v=0.78Cs.

Keywords: *Dynamic fracture.*

References:

[1] A. Livne, E. Bouchbinder and J. Fineberg, "The breakdown of linear elastic fracture mechanics near the tip of a rapid crack", arXiv:0807.4866 (2008).
[2] E. Bouchbinder, A. Livne and J. Fineberg, "Weakly nonlinear theory of dynamic fracture", arXiv:0807.4868 (2008).

Simultaneous application of creep and relaxation formulations to study nonlinear behavior of particle-reinforced viscoelastic composites

Eyal Levenberg

Postdoctoral researcher, School of Civil Engineering, Purdue University, West Lafayette, Indiana, USA.
Email: elevenbe@purdue.edu

Particle-reinforced viscoelastic (VE) composites exhibit nonlinear time-dependent mechanical behavior. Under pre-peak loading conditions, the bulk strain response is affected by: (i) distributed microcracks originating at the interface between the reinforcing particles and the viscous matrix; (ii) growth and coalescence of preexisting microvoids and microcracks; and (iii) in certain cases, the particulate nature of the material. During strain recovery (after unloading), the mechanical integrity of the material is partially regained as a result of healing of microcracks and closure of microvoids. When the material is allowed to rest for long periods of time, after complete strain recovery had already taken place, additional 'age-stiffening' effects come into play as a result of molecular restructuring and age-hardening of the viscous matrix.

Assuming nonlinearities have an isotropic effect (i.e., the material's symmetry remains unchanged), and considering a one-dimensional loading mode under constant temperature conditions, the following VE creep formulation is deemed appropriate for pre-peak conditions:

$$\varepsilon_c^{ve}(t) = \int_{\tau=0}^{t} D(t-\tau) \cdot d\tilde{\sigma}^{ve}(\tau) \tag{1}$$

in which $\varepsilon_c^{ve}(t)$=computed VE strain; $D(t)$=uniaxial linear VE creep compliance; t=physical time; and τ=time-like integration variable. The effective VE stress $\tilde{\sigma}^{ve}(t)$, is defined as $\tilde{\sigma}^{ve} = \sigma / C^{ve}$ in which σ=applied stress and C^{ve}=a positive scalar entity named 'relative VE stiffness' that links the effective and applied stresses and embodies all nonlinear VE behavior. For a linear material C^{ve} equals unity at all times; in the nonlinear case C^{ve} equals unity only in the pristine state and experiences changes thereafter. Decrease in C^{ve} under load is commonly referred to as 'damage'; increase in C^{ve} during recovery intervals is referred to as 'healing'; increase in C^{ve} during long rest periods represents 'age-stiffening'; and reversible (short term) increase in C^{ve} under sustained compressive loads is referred to as 'stiffening'.

The most desirable method for investigating nonlinear VE behavior is to expose the evolution of C^{ve} directly from an experimental dataset, with minimal assumptions. To accomplish this, an analysis scheme is herein proposed, which utilizes both the creep (Equation 1) and relaxation formulations (Equation 2) simultaneously while retaining their classical interrelationship through the convolution integral. As a first step, an error term is defined to quantify the ability of the creep formulation (i.e., ε_c^{ve}) to match measured VE strains (ε_m^{ve}). Second, the shape of $D(t)$ is expressed mathematically, e.g., using a modified power law. Third, the relaxation modulus $E(t)$ is concurrently calculated from $D(t)$ using usual numerical interconversion techniques. Fourth, the resulting $E(t)$ and ε_m^{ve} are used in the relaxation formulation to calculate $\tilde{\sigma}^{ve}$ throughout the test:

$$\tilde{\sigma}^{ve}(t) = \int_{\tau=0}^{t} E(t-\tau) \cdot d\varepsilon_m^{ve}(\tau) \tag{2}$$

Fifth, both $\tilde{\sigma}^{ve}(t)$ and $D(t)$ are used in Equation 1 to compute ε_c^{ve}. Finally, ε_c^{ve} is compared with ε_m^{ve} to evaluate the error term defined in the first step. At this point the entire procedure is repeated with a new set of parameters for $D(t)$ until a close fit of the data is achieved; this is done using nonlinear optimization techniques. The evolution of C^{ve} is thereafter obtained for loading periods (only) based on the ratio $C^{ve} = \sigma / \tilde{\sigma}^{ve}$. Under complete unloading, both σ and $\tilde{\sigma}^{ve}$ vanish, and C^{ve} cannot be observed.

Asphalt concrete is a composite blend of stiff (elastic) aggregates of a large range of sizes (~95% by weight), relatively soft viscous bitumen (~5% by weight) and air-voids of different sizes (~7% by volume). The aforementioned procedure was applied to study the nonlinear VE response to load of a cylindrical asphalt specimen under constant temperature conditions and various loading modes. The results indicated that (i) 'damage' occured under any type of loading; (ii) partial 'healing' took place during strain recovery intervals; and (iii) the material stiffened when placed under sustained compressive conditions.

As an example, the following figure presents the evolution of C^{ve} for a material specimen exposed to several creep cycles in isotropic compression mode, separated by 1,800 seconds of recovery intervals. Values of C^{ve} (circular markers) are depicted on the left ordinate and the abscissa represents cumulative time under pressure. The results are a little 'noisy' mainly because measured strains are used in Equation 2. Also shown in this figure, on the right ordinate, are the applied confining stresses (solid lines) from which the loading shape during the creep sequences can be observed. It may be seen that C^{ve} changed under load throughout the experiment, indicating nonlinear VE behavior. At the beginning of each creep cycle C^{ve} dropped in value, indicating 'damage'. By comparing the level of C^{ve} at the end of a creep cycle with the level of C^{ve} at the very beginning of the following creep sequence, it may be inferred that C^{ve} also changed during recovery intervals. Finally, it may be seen that under sustained compressive conditions (creep sequences 5 and 6), C^{ve} increased significantly indicating that the material experienced short term stiffening.

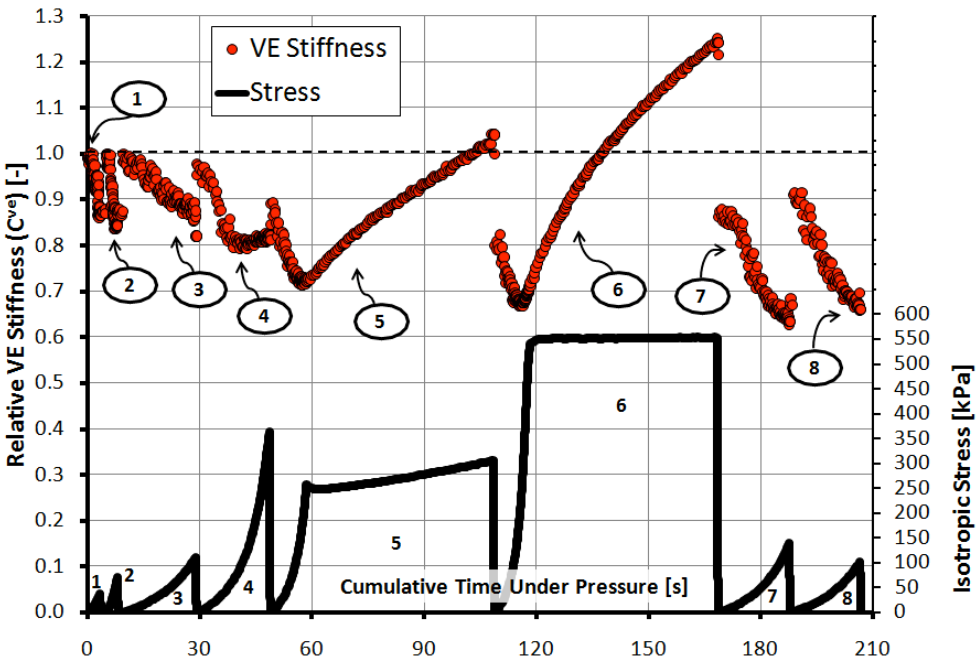

Evolution of C^{ve} and applied confining stress history vs. cumulative time under pressure.

Keywords: Viscoelasticity, Damage, Healing.

References:

[1] Levenberg, E. (2006), "Constitutive modeling of asphalt-aggregate mixes with damage and healing, " Ph.D. Dissertation, Technion - Israel Institute of Technology, Haifa, Israel.

[2] Levenberg, E. and Uzan, J. (2007), "Uniqueness of the viscoelastic time-function for asphalt-aggregate mixes, " Proceedings of the International Conference on Advanced Characterization of Pavements and Soil Engineering Materials, Vol. 1, pp. 35-48.

[3] Park, S.W. and Schapery, R.A. (1997), "A viscoelastic constitutive model for particulate composites with growing damage, " International Journal of Solids and Structures, Vol. 34(8), pp. 931-947.

[4] Park, S.W. and Schapery, R.A. (1999), "Methods of interconversion between linear viscoelastic material functions. Part I - a numerical method based on Prony series, " International Journal of Solids and Structures, Vol. 36(11), pp. 1653-1675.

[5] Smith, T.L. (1971), "Empirical equations for representing viscoelastic functions and for deriving spectra, " Journal of Polymer Science, Vol. 35(Part C: viscoelastic relaxation of polymers), pp. 39-50.

[6] Uzan, J. and Levenberg, E. (2007), "Advanced testing and characterization of asphalt concrete materials in tension, " International Journal of Geomechanics, Vol. 7(2), pp. 158-165.

Analyzing transient turbulence in a stenosed carotid artery by Proper Orthogonal Decomposition

Leopold Grinberg[1], Alexander Yakhot[2], George Em Karniadakis[1]

[1]Division of Applied Mathematics
Brown University Providence, RI 02912, USA
[2]Department of Mechanical Engineering,
Ben-Gurion University, Beersheva 84105, Israel
Email: yakhot@bgu.ac.il

Atherosclerotic plaques inside an arterial wall result in a local occlusion of the artery lumen - a stenosis. The stenosis may trigger transition to turbulence and the onset of turbulence downstream of severe occlusions has been observed in the laboratory experiments. We employ Computational Fluid Dynamics (CFD) to investigate blood flow in a carotid artery, which has an occlusion in the cross-section area of its internal branch. Flow in a stenosed carotid artery has been studied experimentally and numerically by many authors. We have performed *model-free* three-dimensional direct numerical simulations (DNS) of flow through a carotid artery. A geometric model of the carotid artery was obtained from *in-vivo* MRA images shown in figure. In this study, we apply the Proper Orthogonal Decomposition (POD) to analyze pulsatile transitional laminar-turbulent flows in a carotid arterial bifurcation. We use high-accuracy CFD results to demonstrate the possibility of analyzing transient turbulence in a stenosed carotid artery by POD. Specifically, we use a mesh with 22,441 tetrahedral elements of 7 variable size, and eights-order polynomial approximation (P = 8) within each element, corresponding to 24,685,100 degrees of freedom per one variable. The total number of quadrature points in the computational domain was above 37 millions. Our simulations confirm that a turbulent state appears during the systolic phase of the cardiac cycle and is localized in the post-stenotic region, with relaminarization occurring further downstream of the stenosis. The possibility to extend the POD analysis to routine clinical tests carried out by ultrasound medical imaging techniques has been analyzed and discussed.

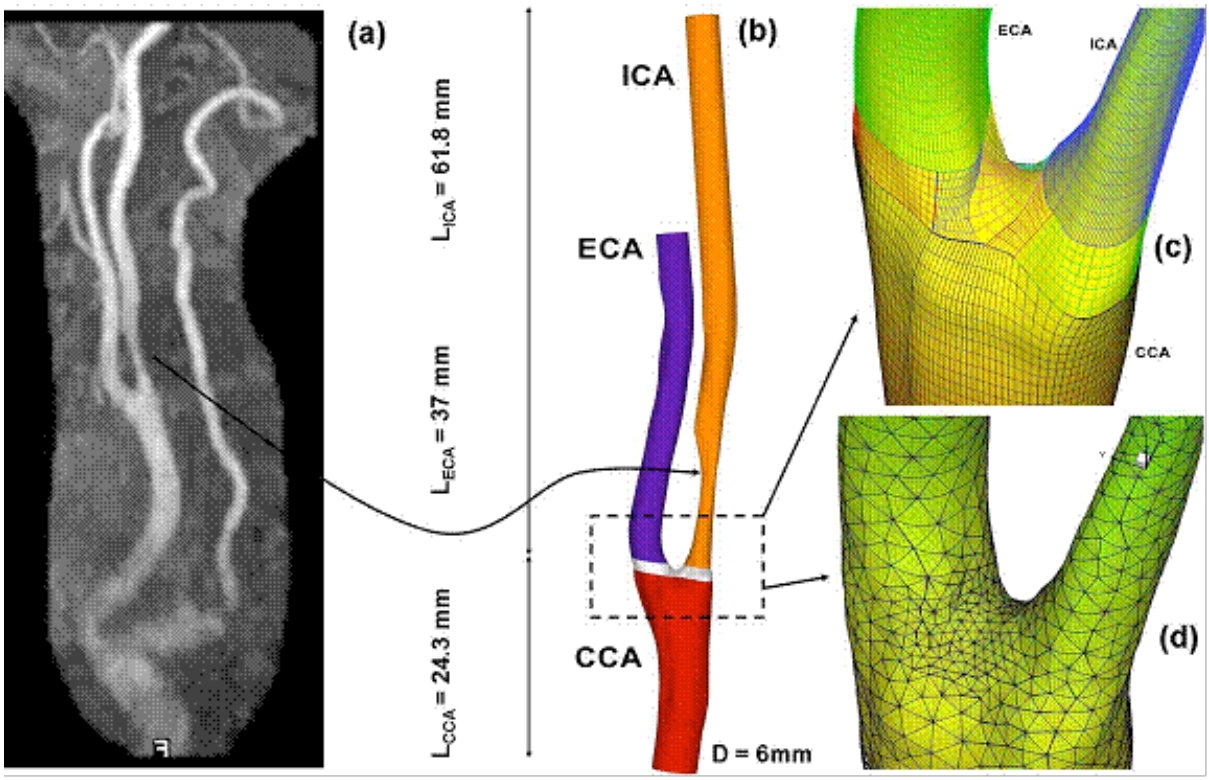

Rogue (freak) waves in ocean and in a laboratory tank

L. Shemer

School of Mechanical Engineering, Tel-Aviv University
Tel-Aviv 69978, Israel. E-Mail: shemer@eng.tau.ac.il. URL: http://www.eng.tau.ac.il/~shemer/

Rogue, or freak waves, are large waves that appear locally and spontaneously in the sea. Usually waves with heights exceeding twice the significant wave height are considered to belong to this category. When such waves appear in a stormy sea, they can pose a threat to large ships and off-shore platforms. The frequency of appearance of those waves therefore constitutes an important design parameter in marine and off-shore engineering. There are numerous indications that this frequency seems to be considerably larger than expected for a random Gaussian sea. The talk addresses two aspects of rogue waves' investigation in a laboratory wave tank: i) development of a method to generate single very high wave at a prescribed location in a tank to enable experimental study of interactions of those waves with structures; and ii) investigation of rogue wave properties in a random wave field.

In the present study deterministic high waves are generated by nonlinear focusing process in which a single unidirectional steep wave emerges from an initially wide amplitude- and frequency-modulated wave group at a prescribed position in the laboratory wave tank. This phenomenon is studied both theoretically and experimentally. The spatial version of the Zakharov equation is applied in the numerical simulations. Experiments were carried out in the Large Wave Channel in Hanover, which is 330 m long, 7 m deep (filled to the mean water depth of 5 m) and 5 m wide. Instantaneous surface elevation was simultaneously measured by 25 resistance-type wave gauges distributed along the tank. The surface elevation $\zeta(t)$ at the focusing location set at the distance of x=120 m from the wavemaker was prescribed to have the Gaussian envelope

$$\zeta(t) = \zeta_0 \exp(-t/mT_0)^2 cos(\omega_0 t) \qquad (1)$$

Here $\omega_0=2\pi f_0 =2\pi/T_0$ is the carrier wave circular frequency, ζ_0 is the maximum wave amplitude in the group, and the parameter m defines the width of the group. Two values of the carrier wave period, T_0=2.8 s (corresponding to carrier wave length λ_0=12 m), and T_0=4.34 s (λ_0=25 m) were used. The spectrum of (1) also has a Gaussian shape with the relative width at the energy level of half of the maximum that depends on the parameter m. The value of m=0.6 that yields wide spectrum was selected in those experiments. To compute the required driving signal, the Zakharov equation was integrated backwards from the focusing location to the wavemaker at x=0. The maximum possible wave steepness within the group $\varepsilon = \zeta_0 k_0$ is adopted as the measure of nonlinearity of the wave field. Experiments were carried out for the values of ε up to 0.3. The output voltages of all wave gauges were sampled at frequency of 40 Hz/channel for the total sampling duration of 400 s, sufficient for the wave field excited by the wavemaker to propagate beyond the last wave gauge. Good agreement between experiments and calculations is demonstrated in Fig. 1.

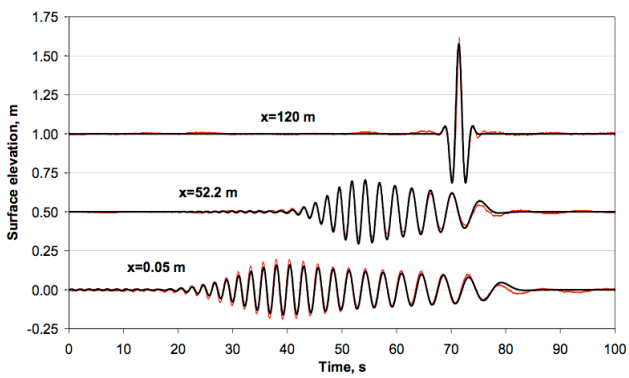

Figure 1. Wave group evolution along the tank for T_0=2.8 s. Black line-computations, red line – measurements.

Random wave field studies were based on the spectrum of the surface elevation variation at the wavemaker also given by (1). All experiments were carried out for the carrier wave period T_0=1.5 s, corresponding to the wave length λ_0=3.51 m. In these experiments, numerous realizations of a wave field that all have identical initial frequency power spectra for the free wave components, but random frequency components' phases in each realization, are generated, and its spatial evolution studied. The value of the spectral width parameter in the present experiments was selected to be m=3.5, yielding a quite narrow spectrum with $\Delta\omega/\omega_0$=0.054. The

discrete frequency spectrum is calculated for the total duration of a single group of 51.2 s so that the frequency resolution of the spectrum Δf is better than 0.02 Hz. The spectrum of (1) was then truncated to leave 60 harmonics around the carrier frequency $f_0=1/T_0$ containing all components with non-negligible amplitudes. For each selected realization of the surface elevation variation at the wavemaker, the amplitude of each spectral component is assigned a random phase. This signal was actually repeated three times, yielding three nearly identical wave groups with the total extent of 153.6 s. Windowing was used to eliminate finite wavemaker displacement at the beginning and the end of the wave excitation period. A single sequence of 3 nearly identical wave groups was excited in each experimental run. The run started only when the water surface was quiescent.

Initial runs performed with ε=0.3 showed occasional wave breaking within the tank. Since the wave breaking is not accounted for in the conservative wave models, it was decided to run most experiments for ε=0.25, with no essential breaking phenomena, and to estimate the effect of nonlinearity on the basis of a limited number of realizations for ε=0.2. The total number of experimental runs in this study is 69 (Series A contained 10 experimental runs at ε=0.2, Series B 46 runs at ε=0.25, and Series C 13 runs at ε=0.3).

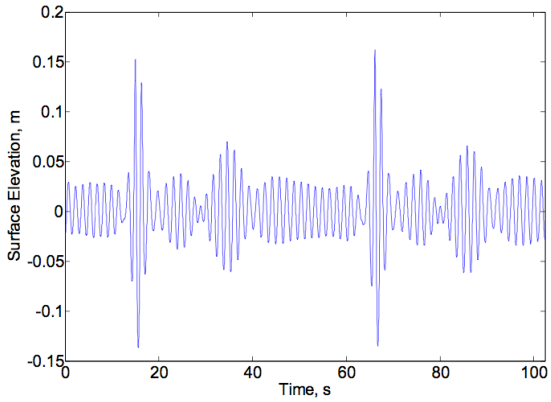

Figure 2. Record of surface elevation variation featuring two nearly identical extreme events (Series B, x=132 m).

In the example of the recorded wave field shown in Fig. 2, two nearly identical wave groups are seen. Each group contains an extreme event with the maximum wave height exceeding the significant wave height by a factor of about 2.5.

Spatial evolution along the tank of the random wave field and its statistical characteristics is studied. It is demonstrated that the probability of extreme events varies significantly with the distance x from the wavemaker and may indeed exceed significantly the values predicted by the Rayleigh distribution. The stronger nonlinearity leads to higher probability of appearance of extremely high wave crest. The stronger is the nonlinearity, the shorter is the distance from the wavemaker at which the probabilities of extremely high wave heights and wave crests attain maximum. This result is consistent with ε^2scaling of the characteristic nonlinear evolution scales.

The variation of additional wave field parameters along the field is studied, including the wave frequency spectra, the higher order statistical moments and the probability density function of wave heights as well as of wave crests and troughs. All these results suggest spatial recurrence of the random wave field. In particular, the high probability of extreme events is closely related to the width of the free wave part of the spectrum. The initial narrow spectra undergo widening, attain maximum width and then get narrower again. The maximum values of the surface elevation kurtosis, as well as maximum deviations of the probability density functions from the Rayleigh distribution all occur at those locations along the tank that are characterized by a relatively wide spectrum.

Transition to turbulence through decline of viscosity

KY Volokh

Faculty of Civil and Environmental Engineering, Technion - Israel Institute of Technology
Haifa 32000, Israel. Email: cvolokh@tx.technion.ac.il URL: http://www.technion.ac.il/~cee/volokh/

Experiments (Mullin and Kreswell, 2005) show that the transition to turbulence can start at Reynolds numbers lower than it is predicted by the linear stability analysis – the subcritical transition to turbulence. To explain these observations qualitatively we suggest that the onset of the subcritical instability is related to decline of viscosity of the fluid: friction between fluid layers fails with the increase of the velocity gradient. To describe the decline of friction theoretically we relax the assumption of the stability of the fluid material and introduce a constant of *fluid strength*, ϕ, in the constitutive equation for the viscous stress:

$$\tau_{ij} = 2\eta\, d_{ij} \exp(-d_{mn} d_{mn} / \phi^2) ,$$

where η is a viscosity constant and $d_{ij} = (\partial_j v_i + \partial_i v_j)/2$ is a symmetric part of the velocity gradient.

The constitutive law is presented graphically in Fig.1 for the shearing flow. The classical Navier-Stokes model is obtained from the enhanced one when the strength goes to infinity.

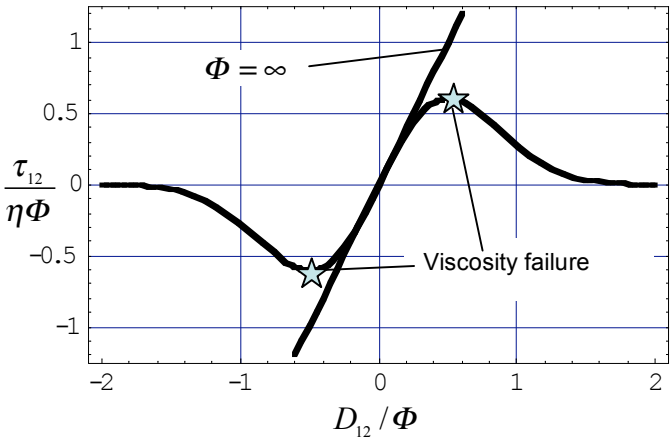

Fig. 1. Viscous stress versus deformation rate in the case of shear flow with finite and infinite strength.

We use the modified Navier-Stokes model to analyze the Couette flow between two parallel plates and find that the lateral perturbations can destabilize the flow and the critical Reynolds number is proportional to the fluid strength. The latter means that the classical Navier-Stokes model of a stable material with the infinite strength does not capture the subcritical transition to turbulence while the modified model does.

Keywords: *Turbulence; subcritical transition; instability; Couette flow; failure.*

Reference:

[1] Mullin, T. and Kerswell, R.R. (eds), 2005. Laminar Turbulent Transition and Finite Amplitude Solutions, Proceedings of the UITAM Symposium, Bristol, UK., Springer, Dodrecht.

Plane stress cavitation in elastic solids

Tal Cohen and David Durban

Faculty of Aerospace Engineering, Technion Haifa 32000, Israel
(T Cohen) Email: btal@tx.technion.ac.il

Cavitation phenomena in nonlinear elastic solids have been studied in the past for spherical and plane-strain cylindrical patterns. The present research attempts to investigate possible cavitation under **plane-stress** conditions with axial symmetry. We consider circular hole expansion under internal pressure and under remote tension. The latter case is of interest in biomechanics in the context of small holes punctured into prestrained soft membrane tissues.

Field equations are formulated with finite strains accounting for severe thickness changes. Material response is modeled by simple Hookean relations of elastic and hyperelastic type. For both constitutive relations a single nonlinear ordinary differential equation is obtained and then solved numerically.

The existence of limiting cavitation stress, for remote tension, has been confirmed for either of the material models. Under internal pressure, however, the applied stress dose not exhibit a saturation level. We shall discuss the specific energy, needed to create a new unit volume of hole expansion, and show for the internally pressurized hole that it does approach an asymptotic value (see figure). That observation may suggest a new definition of cavitation which is based on energy consumption.

Comparison with cavitation stresses for spherical and cylindrical patterns reveals that plane-stress cavitation is attained at lower levels of external tension.